Internalisation of engineered nanoparticles into mammalian cells in vitro: influence of cell type and particle properties

Journal of Nanoparticle Research
An Interdisciplinary Forum for Nanoscale Science and Technology

ISSN 1388-0764
Volume 13
Number 1

J Nanopart Res (2010)
13:293-310
DOI 10.1007/
s11051-010-0030-3

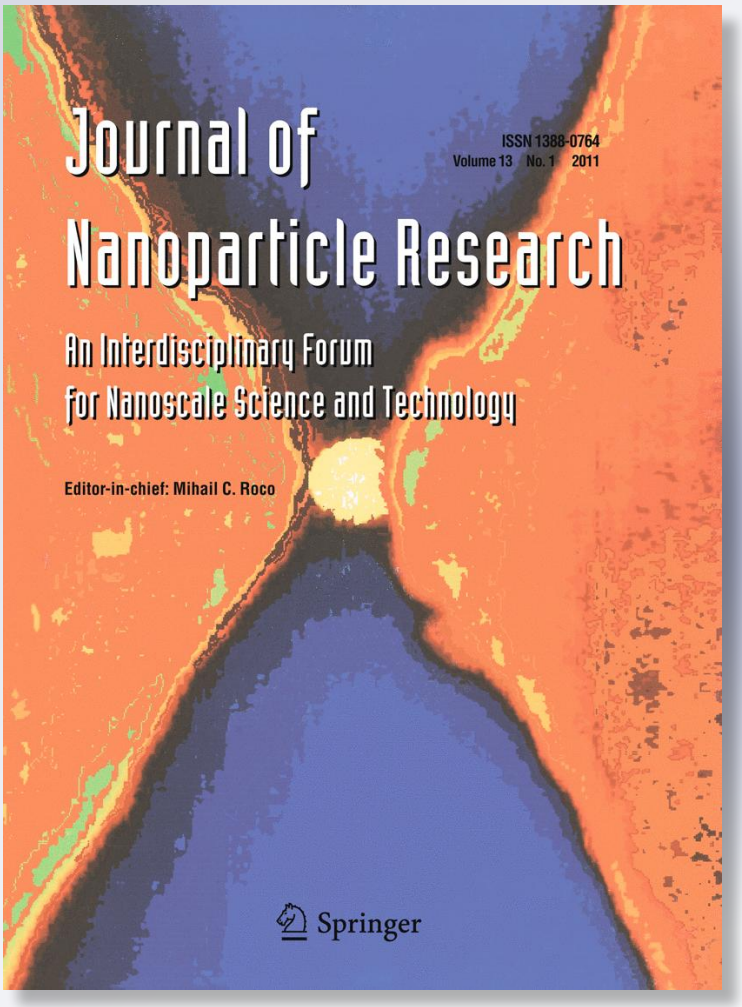

Springer

J Nanopart Res (2011) 13:293–310
DOI 10.1007/s11051-010-0030-3

RESEARCH PAPER

Internalisation of engineered nanoparticles into mammalian cells in vitro: influence of cell type and particle properties

Wibke Busch · Susanne Bastian · Ulrike Trahorsch · Maria Iwe · Dana Kühnel · Tobias Meißner · Armin Springer · Michael Gelinsky · Volkmar Richter · Chrysanthy Ikonomidou · Annegret Potthoff · Irina Lehmann · Kristin Schirmer

Received: 5 May 2010 / Accepted: 7 July 2010 / Published online: 30 July 2010

Abstract Cellular internalisation of industrial engineered nanoparticles is undesired and a reason for concern. Here we investigated and compared the ability of seven different mammalian cell cultures in vitro to incorporate six kinds of engineered nanoparticles, focussing on the role of cell type and particle properties in particle uptake. Uptake was examined using light and electron microscopy coupled with energy dispersive X-ray spectroscopy (EDX) for particle element identification. Flow cytometry was applied for semi-quantitative analyses of particle uptake and for exploring the influence on uptake by the phagocytosis inhibitor Cytochalasin D (CytoD). All particles studied were found to enter each kind of cultured cells. Yet, particles were never found within cell nuclei. The presence of the respective particles within the cells was confirmed by EDX. Live-cell imaging revealed the time-dependent process of internalisation of technical nanoparticles, which was exemplified by tungsten carbide particle uptake into the human skin cells, HaCaT. Particles were found to co-localise with lysosomal structures within the cells. The incorporated nanoparticles changed the cellular granularity, as measured by flow cytometry, already after 3 h of exposure in a particle specific manner.

Electronic supplementary material The online version of this article (doi:10.1007/s11051-010-0030-3) contains supplementary material, which is available to authorized users.

W. Busch (✉) · D. Kühnel
Department of Bioanalytical Ecotoxicology, UFZ-Helmholtz Centre for Environmental Research, Permoserstrasse 15, 04318 Leipzig, Germany
e-mail: wibke.busch@ufz.de

U. Trahorsch · I. Lehmann
Department of Environmental Immunology, UFZ-Helmholtz Centre for Environmental Research, Permoserstrasse 15, 04318 Leipzig, Germany

S. Bastian · M. Iwe · C. Ikonomidou
Department of Pediatric Neurology, University Children′s Hospital Carl Gustav Carus, Technical University of Dresden, Fetscherstrasse 74, 01307 Dresden, Germany

T. Meißner · V. Richter · A. Potthoff
Fraunhofer Institute for Ceramic Technologies and Systems, Winterbergstrasse 28, 01277 Dresden, Germany

A. Springer · M. Gelinsky
Institute for Materials Science and Max Bergmann Center of Biomaterials, Technical University of Dresden, Budapester Strasse 27, 01069 Dresden, Germany

C. Ikonomidou
Department of Neurology and Waisman Center, University of Wisconsin, Madison, WI 53792, USA

K. Schirmer
Eawag, Swiss Federal Institute of Aquatic Science and Technology, 8600 Dübendorf, Switzerland

K. Schirmer
ETH Zürich, Institute of Biogeochemistry and Pollutant Dynamics, 8092 Zürich, Switzerland

By correlating particle properties with flow cytometry data, only the primary particle size was found to be a weakly influential property for particle uptake. CytoD, an inhibitor of actin filaments and therewith of phagocytosis, significantly inhibited the internalisation of particle uptake in only two of the seven investigated cell cultures. Our study, therefore, supports the notion that nanoparticles can enter mammalian cells quickly and easily, irrespective of the phagocytic ability of the cells.

Keywords Engineered nanoparticles · Uptake · Mammalian cells · Flow cytometry · Microscopy · Cytochalasin D · Health and safety

Background

Nanoparticle risk assessment is based on toxicological in vitro and in vivo data and needs to be performed for many different kinds of nanomaterials. These materials differ in their properties, as chemicals do, according to their projected applications. Whereas nanoparticles are modified for medical applications to promote entry into cells, engineered nanoparticles for industrial applications are not designed to do so. Since nanoparticles are close or similar in size to biological entities, such as proteins, DNA or viruses, concerns about the nanoparticles' ability of entering cells and distributing within organisms undesirably are justified. The potential entry of technical nanoparticles into mammalian cells is therefore of special relevance for occupational health.

Several studies have reported toxicological effects of particles upon internalisation by cells (Xia et al. 2006; Gojova et al. 2007; Bastian et al. 2009; Bhattacharya et al. 2009; Papis et al. 2009). Most effects found so far are related to reactive oxygen species, dissolved ions or mixtures of unknown components (e.g. diesel exhaust particles). However, understanding the ability of nanoparticles to enter different kinds of cells is important even in the absence of short-term toxicological effects because particle accumulation, transfer between tissues and mixture effects with chemicals (e.g. drugs, xenobiotics) or biological molecules (e.g. DNA, proteins) may have long-term consequences.

To date, particle incorporation is mostly attributed to phagocytic cells, such as monocytes and macrophages; however, particle uptake by non-phagocytic cells has been reported as well, especially for nanoparticles (Stearns et al. 2001; Chen and von Mikecz 2005; Geiser et al. 2005; Chithrani et al. 2006; Long et al. 2006). While large particles are thought to be taken up by phagocytosis, an actin filament-dependent process, smaller particles seem to be internalised by other endocytic pathways with as of yet no apparent strict size threshold. Rejman et al. (2004) found no uptake of 1000 nm fluorescent microspheres into non-phagocytic cells, whereas the internalisation of 500 nm and smaller microspheres via different endocytic paths was observed. On the contrary, Gratton et al. (2008) demonstrated that particles of 2 and 3 μm were internalised into HeLa cells by different endocytotic pathways. We previously analysed the ability of a rainbow trout (*Oncorhynchus mykiss*) gill cell line (RTgill-W1) to internalise and respond to tungsten carbide (WC) and tungsten carbide cobalt (WC–Co) nanoparticles and found incorporation into the cells irrespective of particle agglomeration state and media composition (Kühnel et al. 2009). These studies indicated that nanoparticles can generally be internalised by cells which are not known to perform phagocytosis.

Since in vitro studies so far mostly focussed on effects and uptake of a special kind of nanoparticle on one population or culture of cells, our approach was to compare several technical nanoparticles regarding their internalisation ability into different mammalian cell cultures. Whether the cell type or particle properties influence the particle uptake was one of the major questions. Therefore, we chose cells of different origin to model exposed organs (based on permanent and primary as well as phagocytic and non-phagocytic cells). Our focus was on technical nanoparticles which are under development for industrial large scale production. Most of the chosen nanoparticles find application in the field of producing hard metals, also called cemented carbides. We investigated six types of engineered nanoparticles (small and large tungsten carbide (WC_S, WC_L), tungsten carbide cobalt (WC–Co), titanium nitride (TiN), titanium dioxide (TiO_2) and diamond), and compared their ability to enter the cells. All particles were characterised regarding their physico-chemical properties and their behaviour in aqueous media

(Bastian et al. 2009; Meißner et al. 2009, 2010; Potthoff et al. 2009). Particle internalisation was confirmed in different ways, including element analysis as part of the electron microscopic characterisation and measurement of changes in side scatter (SSC) values in flow cytometry analyses, as suggested for semi-quantitative determination of particle uptake by Stringer et al. (1995). Finally, Cytochalasin D (CytoD), an inhibitor of actin polymerisation and therewith the function of the cytoskeleton, helped to decipher the involvement of phagocytosis in nanoparticle uptake.

Materials and methods

Sources and initial characterisation of nanoparticles

Six types of engineered nanoparticles which are of industrial and therewith of occupational relevance were selected for this study. WC based particles are widely used in hard metal industries for the production of hard metals and tools. TiN is an extremely hard ceramic material, often used as a coating on titanium alloys, steel, carbide and aluminium components to improve the substrate's surface properties. Metal oxides, such as TiO_2, are frequently used in consumer products, especially as pigments or emery substances in, e.g. sunscreens, toothpaste or paints. Finally, diamond nanoparticles are mainly used as polishing agents for industrial applications. The following nanoparticles, which represent these groups of industrially relevant particles, were investigated in this study: two types of WC nanoparticles with different primary particle size (WC_L, WC_S), WC–Co (10 mass% cobalt content), TiN, titanium dioxide (TiO_2 P25, Degussa Evonik GmbH, Essen, Germany) and diamond (MBM 0-1/2, Diamond Innovations, Dreieich, Germany). WC_L was prepared by a chemical process involving carbothermal reduction and carburisation of WO_3, and disaggregated and mixed, respectively, by means of a ball mill. In contrast, WC_S is a powder material manufactured from coarse WC powder by plasma reactor treatment. WC–Co is a mixture of WC_L and a cobalt powder. Detailed information of preparation and physicochemical characterisation of WC_L and WC–Co are already described elsewhere (Bastian et al. 2009). TiN powder was manufactured by chemical vapour reaction of titanium tetrachloride with ammonia and hydrogen (Naß et al. 1994). TiO_2 and diamond were taken as-received.

The specific surface area of the nanopowders was determined according to Brunauer–Emmet–Teller (BET) using a Micromeritics ASAP 2010 Analyser (Accelerated Surface Area and Porosimetry System, Micromeritics GmbH, Mönchengladbach, Germany) and nitrogen. Phase composition was measured using a XRD7 diffractometer (Seifert-FPM, Freiberg, Germany). Morphology and particle size were verified by scanning electron microscopy (SEM) using a Zeiss LEO FEG (Carl Zeiss SMT AG, Oberkochen, Germany).

Preparation and characterisation of particle suspensions

All particle suspensions were prepared in pure water (resistivity $\geq$ 18 MΩ cm; Wilhelm Werner GmbH, Leverkusen, Germany). For WC–Co, WC_S, TiN and TiO_2, the addition of sodium polyphosphate (Graham's salt; Merck, KGaA, Darmstadt, Germany) was necessary to obtain electrostatic stabilisation of the particles (0.03% (wt/v) for the tungsten based and 0.05% (wt/v) for the titanium based particles). Graham's salt is an often-used dispersant that is non-toxic in the applied concentrations. Diamond particles were suspended in 10^{-4} M KOH to achieve stabilisation of the suspension. The suspensions were treated by probe sonication (UDS 751; Topas GmbH, Dresden, Germany) for deagglomeration. Particle suspensions were sterilised by autoclaving and treated for 15 min in an ultrasonic bath (Merck Eurolab, Darmstadt, Germany) prior to treatment of cells to ensure optimal dispersal. After preparation as well as after autoclaving, we quantified particle size and zeta potential. Zeta potentials were determined by measuring the electrophoretic mobility of the suspended particles (Zetasizer Nano ZS, Malvern Instruments Ltd, Worcestershire, UK). The electrophoretic mobility has been calculated into the zeta potential using the Smoluchowski equation. Particle size and the polydispersity index (PDI) were determined by means of dynamic light scattering using again a Zetasizer Nano ZS.

Cell cultures

In order to compare the behaviour of several kinds of cells regarding the uptake of nanoparticles we choose cell cultures of different origin. The selected cell cultures represent possible primary or secondary exposed organs, e.g. skin, lung, blood system and brain. Thereby we chose well established permanent cell lines, such as the human keratinocytes—HaCaT, the lung epithelial cells—A549, the monocyte cell line—THP1, and the rat oligodendroglial cell line—OLN93. Since especially functions of differentiated brain cells are hardly achievable with permanent cell lines, we also used freshly isolated rat astroglial cultures and separated microglia and astrocytes for our experiments. Moreover, since phagocytic cells are supposed to internalise particles, we included another kind of freshly isolated cells, namely human peripheral blood mononuclear cells (PBMC). These cells consist of two cell populations, lymphocytes and monocytes. The monocyte population is responsible for uptake and digestion of endogenous or foreign particulate material via phagocytosis in the human body. Having included PBMC allowed us to compare the internalisation of nanoparticles between the primary (PBMC) and the permanent (THP1) monocytes.

The handling of all cell cultures, as well as the isolation of the primary cells, was performed according to standard protocols and is explained in detail in supplemental material (Additional file 1).

Exposure of cells to particles

Cells were counted using a hemocytometer. Cells were seeded in 24 well plates (TPP) in a volume of 500 µL (for primary rat brain cells) or in 6 well plates in a volume of 2 mL (for all other cell types) at a density of approximately 1×10^5 cells/mL, and allowed to attach for 24 h before addition of particle suspensions. Numbers of seeded cells varied slightly dependent on exposure time or measured endpoint, but were always the same for biological replicates. Details of cell numbers seeded per experiment are given in supplemental material (Additional file 1). All exposures were carried out in complete cell culture medium containing 10% foetal bovine serum (FBS). We had previously shown that the nanoparticles formed stable aggregates in the presence of bovine serum albumin (BSA) or serum in the exposure suspensions (Bastian et al. 2009; Meißner et al. 2009, 2010; Potthoff et al. 2009).

Dosing was achieved by adding 200 µL (6 well) or 50 µL (24 well) of the respective particle dilution to 1800 µL (6 well) or 450 µL (24 well) of complete cell culture medium to reach final nanoparticle concentrations of 20 and/or 30 µg/mL, the latter being the highest achievable concentration based on limitations in the preparation of particle suspensions. All experiments were repeated for a minimum of four times. Controls of the water or water with supplements used to prepare the particle suspensions were included as appropriate in all experiments. Cells were treated with nanoparticles for 1 h up to 3 days.

Treatment of cells with CytoD

For uptake inhibition experiments, all cell cultures were pre-treated with CytoD (Applichem, Darmstadt, Germany) for 1 h before starting particle exposure. The cell culture medium was changed to the respective media with or without CytoD, using non-toxic concentrations for every cell type as determined in range finding experiments using cell viability indicator dyes. These concentrations were 5 µM for A549, HaCaT, OLN93 cells, primary astrocytes and microglial cells; and 2 µM for PBMC and THP1 cells.

Flow cytometry

After exposure to nanoparticles for 3 and 24 h (with and without CytoD), cells were washed with PBS, carefully detached with Accutase (PAA Laboratories) and again washed two times with PBS. After re-suspending in 200 µL PBS with 10% FBS, cells were measured directly using a flow cytometer (FACS Calibur, Becton-Dickinson, Franklin Lakes, USA). The median SSC values were analysed as a marker for granularity, which increases with particle uptake. For each measurement we counted viable 10^4 cells. Since particle exposure itself affected cell viability in some cases at the highest applied concentrations (30 µg/mL), the gates in flow cytometry data analyses were set to analyse viable cells only.

Cell viability

Cell viability was assessed in independent experiments using standard protocols with fluorescence

(alamarBlue, CFDA, AM) or absorbance (MTT) indicator dyes and a GENios Plus fluorescence reader (Tecan, Grödig, Austria). At the highest applied particle concentration (30 μg/mL), TiN and WC–Co nanoparticles caused toxicity in some cell types of up to 15%, based on alamarBlue and as described in Bastian et al. (2009). In THP1 and PBMC cells, cell viability was found to decline as much as 60% upon exposure to, respectively, WC-Co and WC_S nanoparticles, relying on MTT (3-(4,5-dimethylthiazol-2-yl)-2,5-diphenyltetrazolium bromide).

Electron microscopy

Characterisation of nanoparticle morphology and localisation after incubation was performed with SEM and scanning transmission electron microscopy (STEM). SEM was assessed as previously described (Bastian et al. 2009). Briefly, cells were fixed with 2% (v/v) glutaraldehyde (Serva, Heidelberg, Germany) at room temperature, post-fixed with 1% (v/v) osmium tetroxide (Roth, Karlsruhe, Germany), dehydrated in a graded series of acetone (including a staining step with 1% (v/v) uranyl acetate) and embedded in epoxy resin according to Spurr (1969). Prior to energy dispersive X-ray spectroscopy (EDX), samples were fixed in 2% (v/v) glutaraldehyde, dehydrated and embedded in epoxy resin as above. Samples were cut on a Leica EM UC6 ultramicrotome (Leica, Vienna, Austria), equipped with a diamond knife (Diatome, Biel, Switzerland), carbon coated and analysed using a Philips XL 30 ESEM (Philips, Eindhoven, Netherlands) in SEM mode. For energy dispersive X-ray microanalysis (EDX), we used an EDAX detecting unit and EDAX software (version 3.0; EDAX Inc., Mahwah, NJ, USA).

For STEM investigations, harvested cells were fixed with 2% glutaraldehyde at room temperature, post-fixed with 1% osmium tetroxide, dehydrated in a graduated series of acetone (including a staining step with 1% uranyl acetate) and embedded in epoxy resin (Spurr 1969). Ultra thin sections (about 100–300 nm) of samples were prepared on a Leica EM UC6 ultra microtome with a Diatome diamond knife, mounted on carbon coated copper grids and analysed in a Philips ESEM XL 30 equipped with a STEM-detector system. For EDX analysis, epoxy resin embedded samples were prepared as described for SEM analyses (see above). Ultra thin sections of the samples were analysed in a Philips ESEM XL 30. EDX analysis and elemental mapping was done with an EDAX detecting unit and EDAX software.

Light microscopy (movie in supplementary material)

HaCaT cells were plated at a density of 4×10^5 cells/well in a final volume of 2 mL in a 6 well plate (TPP) and allowed to attach for 24 h before addition of particle suspension. Dosing was achieved by adding 200 μL of the WC_L particle suspension to 1.8 mL of complete cell culture medium to reach the final concentration of 30 μg/mL for WC_L nanoparticles. Starting at that time point, photographs were taken every 10 min during a time period of 2 days using an inverse microscope (Leica DMI 4000B, magnification 200×) with a heated stand (37 °C). The pictures are shown as a time flow movie, which is provided as supplemental material (Additional file 2).

LysoTracker staining and microscopy

For LysoTracker staining, HaCaT and OLN93 cells were seeded into 6 well plates (Falcon/Becton-Dickinson, Heidelberg, Germany) at a density of 10^5 cells/well in a total volume of 2 mL and were allowed to attach for 24 h. The medium was then replaced with particle containing medium. After an exposure time of 3 days, the exposure medium was removed and cells were incubated in 50 nM LysoTracker Red (Invitrogen/Molecular Probes, Karlsruhe, Germany) in growth medium using a total volume of 2 mL/well for 2 h. In order to visualise the position of cell nuclei, cells were counterstained with 1 μM Hoechst 33342 (Invitrogen/Molecular Probes, Karlsruhe, Germany) for the last 5 min of the incubation time. The loading solution was replaced with fresh medium and cells were observed using a fluorescent microscope (Leica DMI 4000B, Wetzlar, Germany) equipped with the appropriate filter sets. LysoTracker Red exhibits red fluorescence (excitation: 577 nm, emission: 590 nm). Hoechst is excited at 350 nm, and emits at a maximum of around 461 nm. Micrographs were recorded using the Leica LSM software package LAS-AF 1.8.0 build 1346.

Statistics and graphs

FACS data were analysed using CELLQUEST software (Becton-Dickinson, Heidelberg, Germany) and the FlowJo Software (version 7.2.2; Tree Star Inc., Ashland, OR, USA). SSC values were converted to percent of control and are presented as mean ± SE. Statistical differences were analysed with Student's *t* test (treatment vs. control; or particle exposed cells without CytoD vs. particle exposed cells with CytoD) using Microsoft Excel (Version 2002). Values of $P < 0.05$ were considered statistically significant. Graphs were generated with GraphPad Prism software (GraphPad Prism version 4.00 for Windows, GraphPad Software, San Diego, CA, USA, www.graphpad.com).

Results

In this study we investigated interactions between a set of different cells and different nanoparticles focussing on the particle uptake. We aimed to compare the uptake behaviour of several cell cultures using particles of diverse sizes and materials. For this purpose we exposed permanent cell lines of potential exposed organs (human lung (A549) and skin cells (HaCaT); human blood monocytes (THP1) and rat brain oligodendroglial cells (OLN93) as well as freshly isolated primary blood and brain cells (human PBMC, rat astrocytes and microglial cells) to technical nanoparticles with a primary particle size range from 10 (WC_S) to 73 (diamond) nm. Stable aggregates or agglomerates of these particles within physiological media ranged in size (average hydrodynamic diameter, x_{DLS}) from 115 (WC_S) to 250 (diamond) nm. Electron micrographs of all powders and physical and chemical properties of the particles are shown in Fig. 1 and Table 1.

Particles are taken up by all cells

By means of light microscopy we observed particle sedimentation to the bottom of cell culture vessels within the first hour of exposure. Over time, particle agglomerates became visible within all cells, forming a typical pattern around the nucleus (see also Fig. 2).

To visualise particle uptake over time in more detail, we photographed HaCaT cells every 10 min upon treatment with WC_L nanoparticles for 2 days. The HaCaT cells were found to be robust and well sustain cultivation outside the incubator for up to 48 h without additional buffering or humidity and were therefore chosen for this experiment. About 3 h after particle addition, cells performed visible movements leading to incorporation of particles. Areas around the cells were apparently devoid of particles after 2 days and dark areas appeared inside the cells. It was also seen that some larger particle agglomerates were not taken up by the cells and remained in the media. Particle uptake had no obvious influence on cell division; it was further observable after particle incorporation. (Movie is provided as supplemental material—additional file 2.)

All particles were found within the cytoplasm as demonstrated by STEM (shown exemplarily in Figs. 4 and 6; and Bastian et al. 2009). Corresponding to the light microscopy results, different particles built similar patterns within the cells. To confirm the respective nanoparticles within the cells, we performed EDX analyses and found the corresponding elements of the applied nanoparticles. In case of diamond, EDX analyses were not possible because of the high carbon background. Therefore, the identification of individual nanoparticles or agglomerates in or on cells had to rely on morphologic characteristics of the diamond nanoparticles.

Particles co-localise with lysosomal structures

In order to shed light on the localisation of particles within cells, we used a fluorescent dye (LysoTracker Red) to stain lysosomal structures of particle exposed and control cells, focussing on a subset of cell lines, namely HaCaT, OLN93 and A549 cells. Figure 2 exemplarily shows that dark particle spots did co-localise with LysoTracker positive structures appearing in HaCaT and OLN93 cells after 3 days of exposure to WC–Co and TiN particles, respectively. This indicates a deposition of particles in the lysosomal compartments. This co-localisation was observed in A549 cells as well and was similar for the other types of nanoparticles (data not shown).

Particle uptake changes cellular granularity

Incorporated nanoparticles change the SSC signal standing for the granularity of cells in flow cytometry

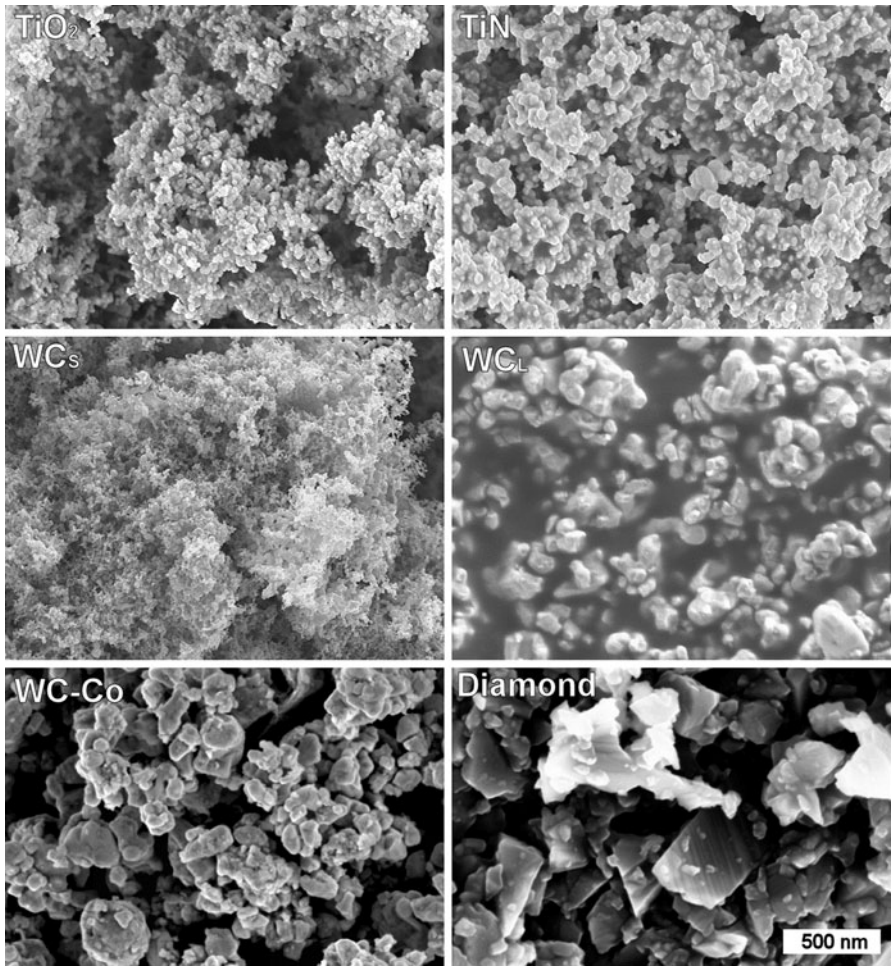

Fig. 1 Electron micrographs of different nanoparticles. SEM images of TiO_2, TiN, WC_S, WC_L, WC–Co and diamond (magnification: ×50,000)

Table 1 Summary of physical parameters of the investigated particles

Particles	Crystalline phase	BET (m^2/g)	x^a_{BET} (nm)	x_{DLS} (nm)	Zeta potential (mV)
TiO_2	Anatase/rutil 80%/20%	55.9	27	170	−50[b]
TiN	Titanium nitride	42.0	26	160	−50[b]
WC_S	Tungsten subcarbide	43.2	9	115	−45[b]
WC_L	Tungsten carbide	6.9	56	145	−35[c]
WC–Co	Tungsten carbide + cobalt	6.6	62	145	−50[b]
Diamond	Diamond	23.3	73	250	−40[d]

Note: Polydispersity index of the investigated particles was below 0.2 (on a scale of 0–1) in all cases, indicating small particles size distributions

[a] Values were calculated assuming the theoretical density of the powders; particles were suspended in water with [b] Graham's salt or [c] Water or [d] 10^{-4} M KOH

analyses. We found that these changes differ significantly between cell types and particles. Strongest uptake of nanoparticles was found within the monocyte population of primary PBMC. These cells showed a strong time-dependent increase in the SSC signal, exemplarily shown for the WC_L particles in Fig. 3. Interestingly, the SSC signal for lymphocytes, a secondary cell type within the primary

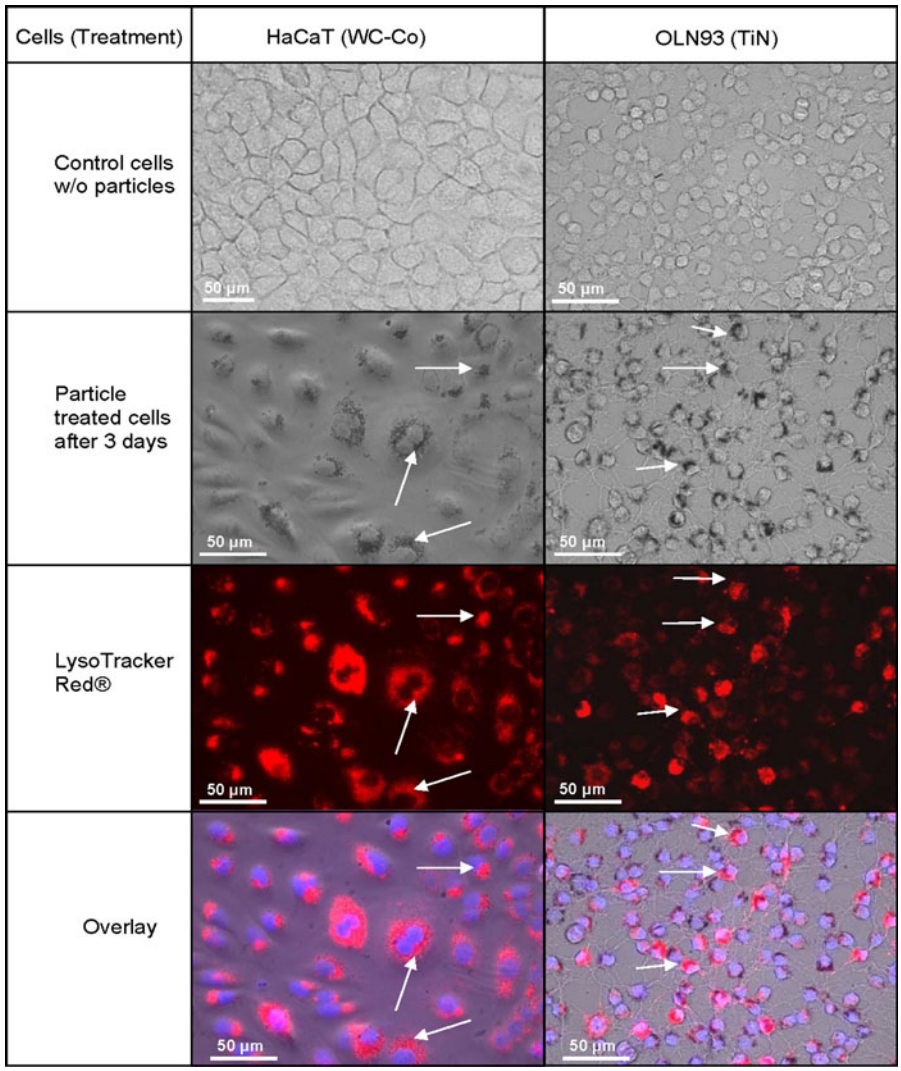

Fig. 2 Light and fluorescent microscopy images of HaCaT and OLN93 cells exposed to WC-Co and TiN nanoparticles for 3 days. Cells were stained with the fluorescent dyes LysoTracker Red® (lysosome marker) and Hoechst 33342 (staining of cell nuclei). Particle agglomerates form specific patterns around the cell nuclei visible in transmission light pictures. Staining of cells with LysoTracker Red® indicates the distribution of lysosomes which co-localise with the particle patterns as demonstrated in the overlay (magnification: ×400)

culture, was not influenced by particles. Indeed, SEM identified WC_L particles exclusively in monocytes but not in lymphocytes after 24 h of exposure (Fig. 4).

Uptake of nanoparticles was likewise observed in all other cell types (and was statistically significant compared to respective controls), but was much less compared to the primary monocytes. This is illustrated again for WC_L particles in Fig. 5a. The SSC signal increased about sixfold for primary monocytes and about twofold for all other cell types compared to the respective untreated cells. Surprisingly, the values of the monocyte cell line, THP1, which is assumed to have phagocytic activity (Reyes et al. 1999), were dissimilar to primary monocytes and rather in the range of the other cell types. Exposures to the same mass concentration of WC_S particles (WC with a sixfold smaller primary particle size, but almost similar size of particle aggregates; Table 1) led to a much lower increase of the SSC signals in all cell types (Fig. 5b).

The SSC signals generally increased with particle mass concentration for all types of particles (data not shown). However, for same exposure times and mass concentrations, SSC signals differed and did so more between particle types than between cells (with the exception of primary monocytes). To demonstrate these differences, we exemplarily show the results for the OLN93 cell line after 3 h of exposure to 20 µg/mL of particles (Fig. 6). A slight increase of cellular granularity was found for WC_S and TiN particles;

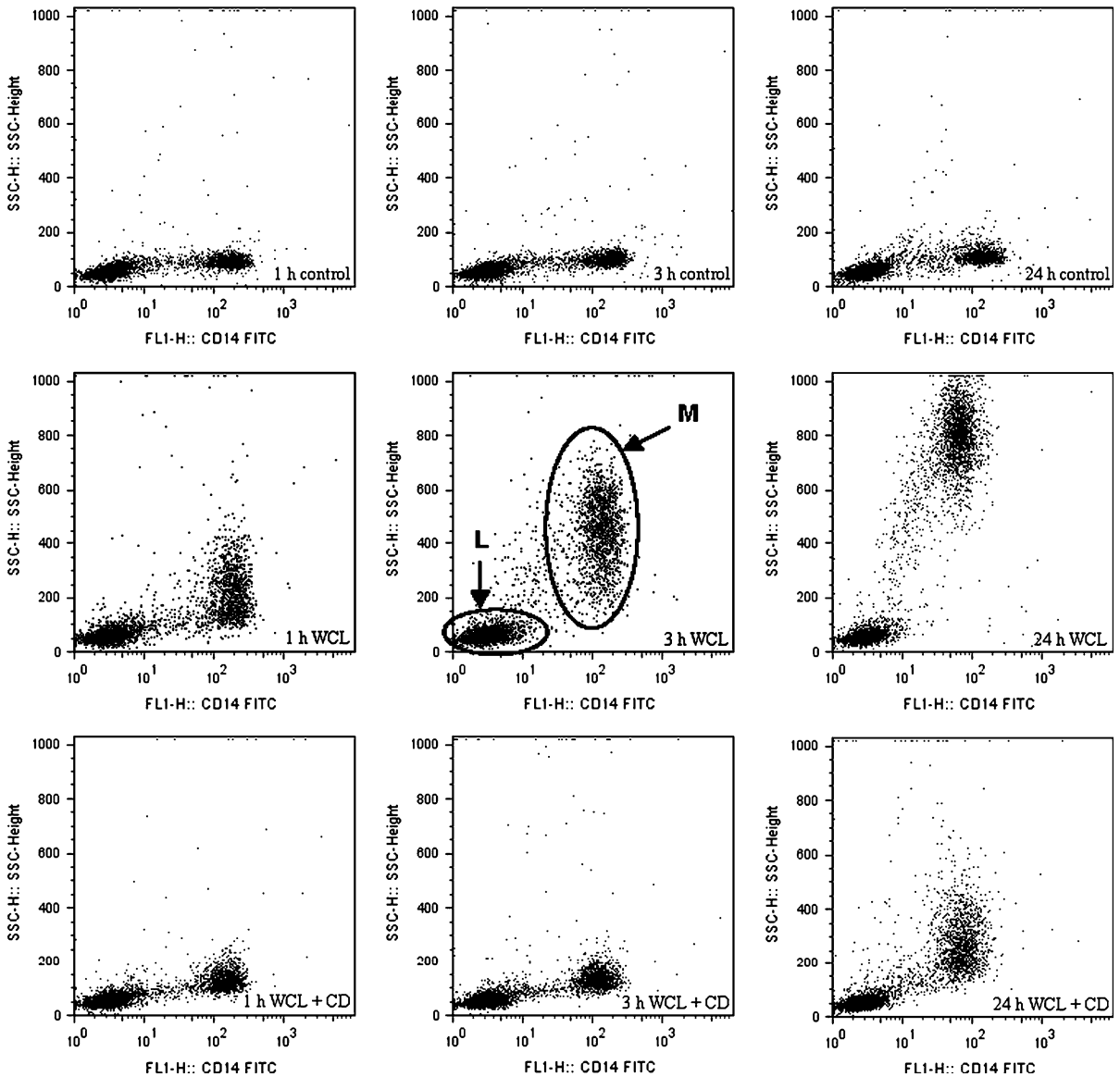

Fig. 3 Uptake of WC_L nanoparticles by PBMC cells after 1, 3 and 24 h of exposure to 30 μg/mL WC_L determined by flow cytometry analyses. PBMC consist of two cell type populations, monocytes (*M*) and lymphocytes (*L*) (exemplarily marked in the middle graph). SSC values of the monocyte cell population increased in a time-dependent manner (*middle panel*) compared to untreated control cells (*upper panel*). The uptake is inhibited when cells are pre-treated with CytoD (2 μM) (*lower panel*). No differences of the SSC signals were detected for the lymphocytes, the second cell population in the primary culture, for any of the treatments

TiO_2, WC_L and WC–Co caused almost equal increases in SSC signals; and diamond particles induced the strongest changes of the granularity (Fig. 6). This pattern was maintained overall after 24 h of exposure with the exception of TiO_2, which exhibited changes in SSC signals closer to diamond than to WC_L and WC–Co particles at this time point (see also Fig. 9).

CytoD indicates involvement of actin filaments in particle uptake for only a few of the investigated cell cultures

We used CytoD to determine whether the destabilisation of actin filaments, which are essential for phagocytosis, influences the ability of cells to

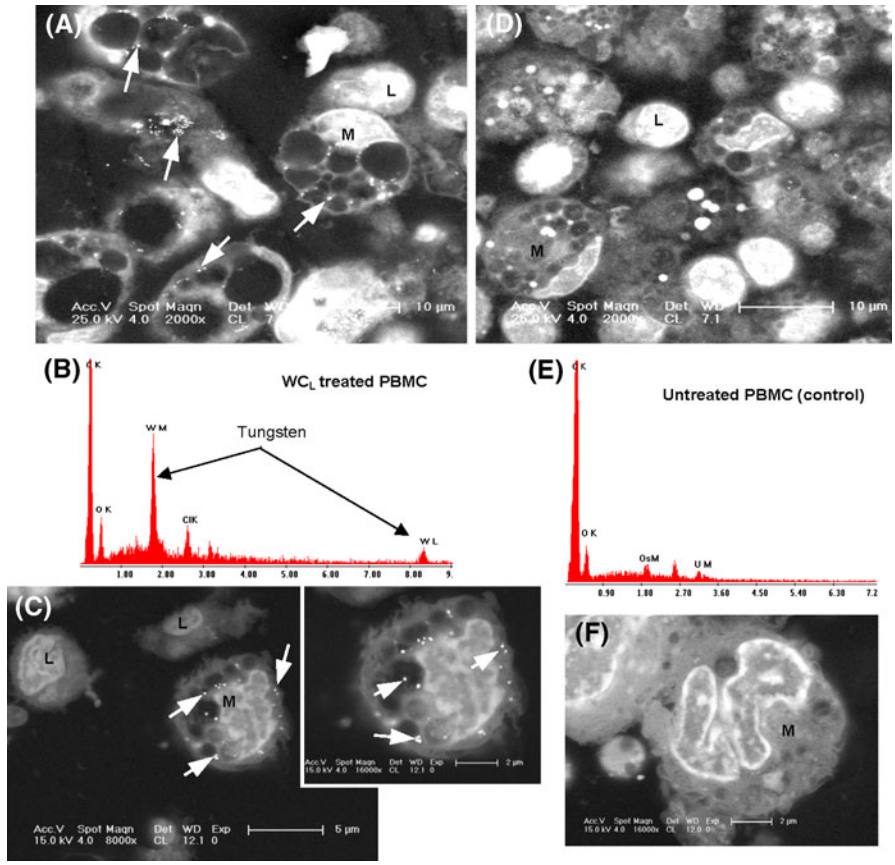

Fig. 4 Scanning electron micrographs of embedded PBMC cells after 24 h of incubation with 30 µg/mL WC_L nanoparticles (**a**, **c**) and with particle free medium (control, **d**, **f**). Heavy elements (e.g. tungsten) appear as light areas (*arrows*), which are concentrated within the monocytes [M] but were not found within lymphocytes [L] (**c**). The EDX spectrum of these light spots shows two prominent peaks with the characteristic energy for X-ray quants originating from the W-M_α (WM) and W-L_α (WL) atomic shells, respectively (**b**). No WC was detected in untreated PBMC (**e**). Other peaks represent further elements in the measured area and are due to compounds of the embedding media (ClK, chloride K_α; OK, oxygen K_α), coating (C, carbon K_α) or staining (OsM, osmium M_α and UM, uranium M_α) (**b**, **e**). Additionally, an intense enlargement of vesicles in monocytes was observed after particle exposure

incorporate the nanoparticles and found that an inhibition of uptake is dependent on the cell type. Strongest inhibitory effects with CytoD were observed for primary monocytes (Fig. 3, bottom row of graphs). Nevertheless, uptake of WC_L particles was significantly inhibited in OLN93 cells as well (Fig. 5a). As with the WC_L particles, the SSC signals of WC_S treated cells were inhibited significantly by CytoD in primary monocytes. Slight inhibitory effects were observed for OLN93, THP1 and microglia cells (Fig. 5b). A significant inhibitory effect of CytoD on particle internalisation was never found for astrocytes, A549 and HaCaT cells.

The inhibitory effect of CytoD on OLN93 cells was observed already after 3 h of exposure and is demonstrated for all investigated particles in Fig. 7a. Preincubation of OLN93 cells with CytoD reduced the changes of the SSC signals for all particles by more than 10% although these changes were statistically significant only for the treatments with WC–Co and diamond particles. Interestingly, SSC signals of primary astrocytes increased particle type dependent in a similar manner as for OLN93 but CytoD had no impact on particle uptake into astrocytes (Fig. 7b).

By SEM coupled with element analysis we confirmed the differences in the inhibitory effect of CytoD using independent samples. Figure 8 shows

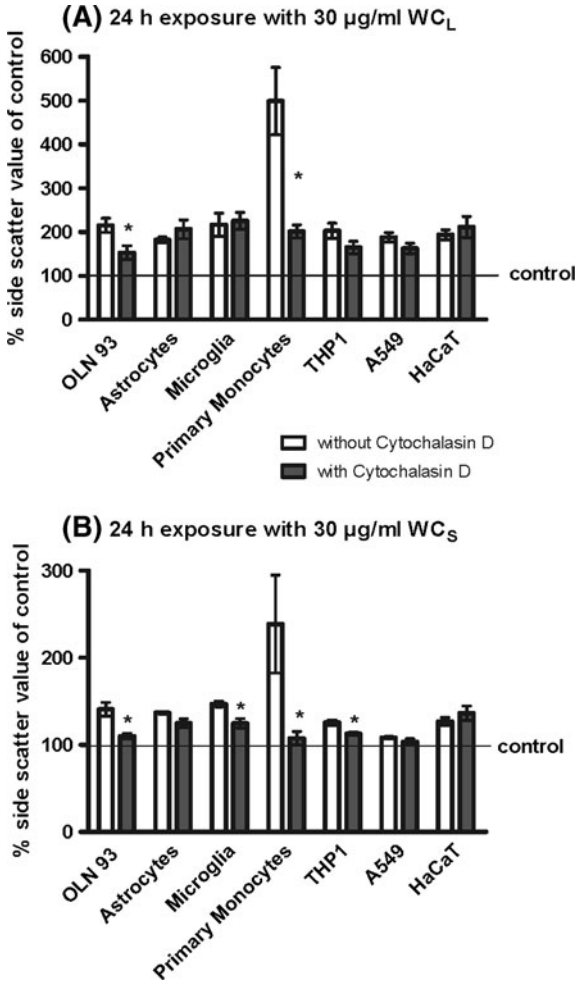

Fig. 5 Relative SSC values after exposure to WC_L and WC_S nanoparticles with and without CytoD pre-incubation. Changes of cellular granularity (measured as SSC) are shown for the different cell types exposed to 30 µg/mL of **a** WC_L and **b** WC_S nanoparticles for 24 h without and with CytoD pre-incubation. *Bars* represent means ± SE as percent of the respective control ($n \geq 4$). SSC values were significantly different from control (cells without particles) as analysed with Student's *t* test for all treatments with the exception of A549 cells treated with WC_S and CytoD ($P < 0.05$); significance of CytoD inhibition is indicated in the graph by the *asterisk* (* $P < 0.05$) and was analysed by Student's *t* test (particle exposed cells without CytoD vs. particle exposed cells with CytoD)

WC_L particles within OLN93 cells and primary astrocytes after 3 h of exposure. As found with the flow cytometry analyses, qualitative analyses of several (randomly chosen) pictures revealed fewer WC_L particles within OLN93 cells pre-treated with CytoD compared to OLN93 cells without inhibitor pre-incubation. Again, uptake of WC_L particles appeared to be inhibited by CytoD only in OLN93 cells but not in astrocytes: similar amounts of WC_L particles were found in several pictures of astrocytes with and without CytoD pre-incubation. This is again in concurrence with data from cytometric analyses.

Role of particle properties in uptake by cells

By comparing changes in cellular granularity between different cell and particle types it became obvious that differences were greater between the different particles than between the cell cultures. In order to analyse which particle properties are responsible for these particle specific changes of SSC values at same particle concentrations, we tried to correlate several physical particle characteristics (surface area, mass, particle number, primary and aggregate particle size, charge and material density, Fig. 9a) with relative SSC outcomes by multiple regression approaches. For these analyses, we added results of another particle type (magnetite) that was investigated in an earlier study (Hildebrand et al. 2009) and merged the mean SSC values for each particle type over four different cell cultures (A549, HaCaT, OLN93 and astrocytes) (Fig. 9b). As mentioned above, the smallest SSC values were expressed with WC_S and the largest with diamond particles. Cellular granularity increased after 24 h in cells exposed to magnetite, TiO_2 and diamond compared to the values after 3 h. Statistical significance was only achieved with TiO_2. However, by comparing particle properties with SSC values we found none of the properties to directly correlate with SSC values, with one exception. After 3 h of exposure, we found a trend towards increasing SSC values with increasing primary particle size (x_{BET}) (Fig. 9c). Yet, this trend was no longer detectable after 24 h, since especially TiO_2 caused much higher values of SSC intensities after 24 h.

Discussion

Our study showed that all nanoparticles were taken up by cells within the first hour of exposure, irrespective of the particle or cell type. In agreement with earlier studies, we found that uptake positively correlated with particle concentration (Stringer et al. 1995; Bao et al. 2007; Gojova et al. 2007; Haberzettl

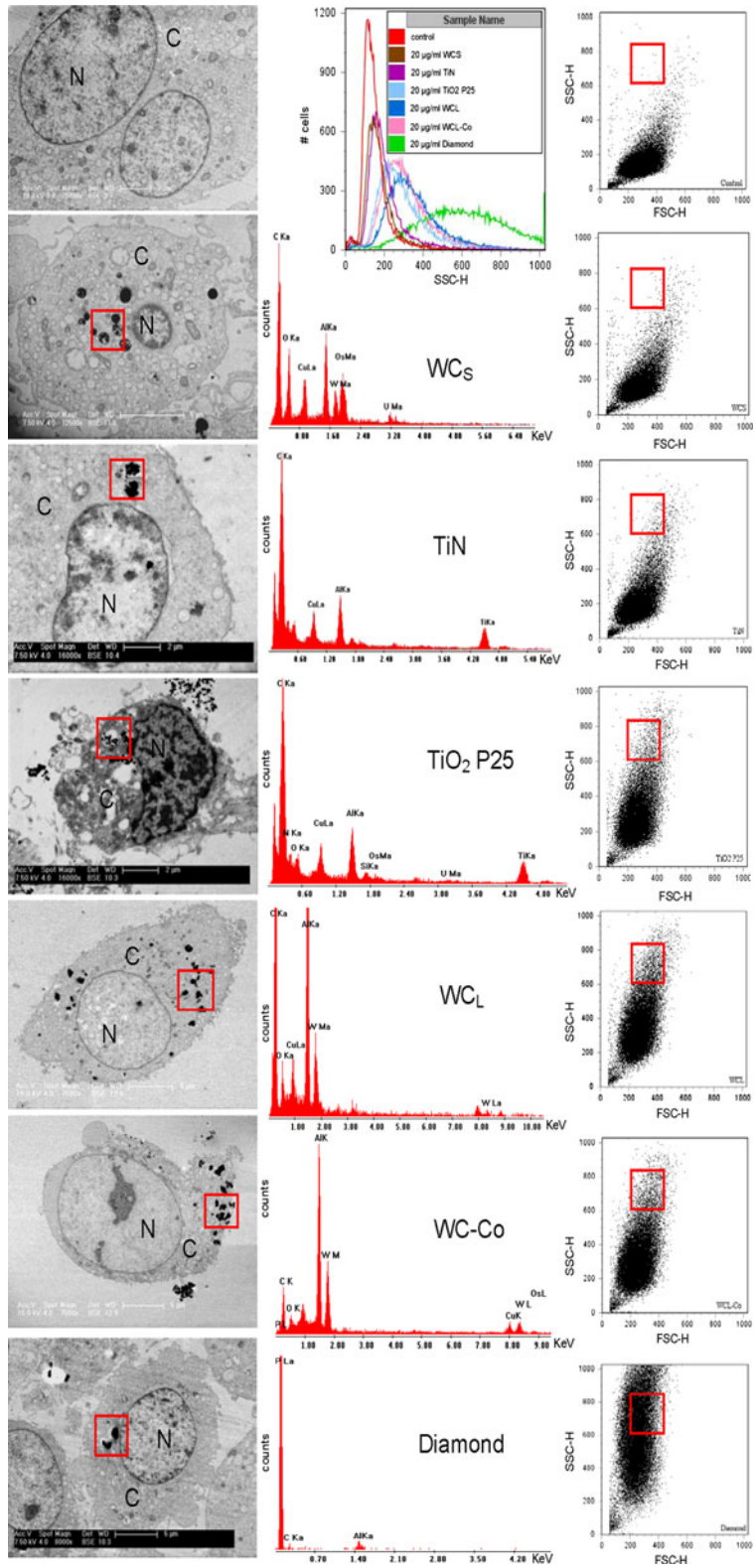

Fig. 6 Electron micrographs and flow cytometry data of OLN93 cells exposed to six kinds of particles. STEM investigations coupled with EDX analyses revealed all types of nanoparticles within the oligodendrocyte cell line OLN93 already after 3 h of exposure (20 µg/mL for each particle type). The *top left* micrograph shows a control cell without particles, the micrographs organised in the column below show incorporated nanoparticles within the cytoplasm (*C*); no particles were found in the nuclei of cells (*N*). EDX analysis was performed for each sample for a respective area (*rectangle*). The spectra, shown in the *middle column*, indicate the elements found within such an area. Graphs of the *right column* show the original data from flow cytometry analyses and reveal different SSC values after the exposure with the same concentration (20 µg/mL) of different nanoparticles. Differences of SSC value distributions over the cell population depending on the particle type are summarised in the *top middle* graph

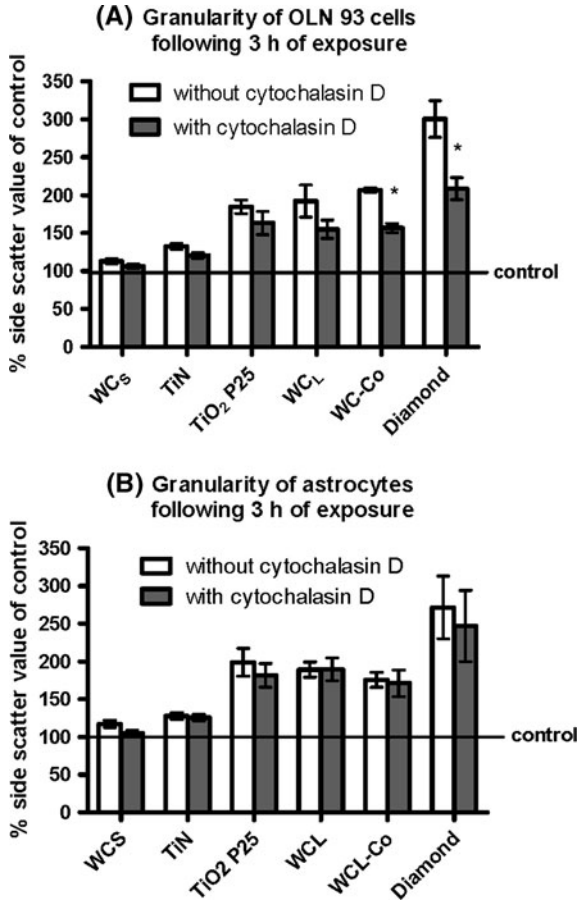

Fig. 7 OLN93 cells (**a**) and primary astrocytes (**b**) were treated with different nanoparticles (20 μg/mL) with and without CytoD pre-incubation. *The bars* represent the changes of cellular granularity (measured as SSC values) after 3 h as mean percent of control (mean ± SE, $n = 4$). SSC values were significantly different from control (cells without particles) as analysed with Student's t test for all treatments with exception of OLN93 treated with WC_S ($P < 0.05$); significance of CytoD inhibition is indicated in the graph by the *asterisk* (* $P < 0.05$) and was analysed by Student's t test (particle exposed cells without CytoD vs. particle exposed cells with CytoD)

et al. 2007). All particles in our study had a negative (anionic) surface charge but otherwise varied with respect to particle size and composition. Uptake was confirmed in several ways, including elemental analysis for the different particle types in cell probes. Overall, we found that the particle type had a greater impact on particle internalisation, as judged by changes of cellular granularity, than the cell type. However, differences between the cell cultures were detected by the use of an actin filament inhibitor, indicating the involvement of different mechanisms of particle uptake in the different cell types.

Electron microscopy studies revealed the intracellular localisation of nanoparticles in the cytoplasm; given the detection limits of our system, we never found particles within the nuclei of cells. This observation is reminiscent of our previous work on WC/WC–Co nanoparticles in various vertebrate cells (Bastian et al. 2009; Kühnel et al. 2009). Higher resolution frequently showed particles to be enclosed in an intracellular membrane. Since these regions co-localised with vesicles indicated by fluorescent tracker as lysosomes, we postulate that the majority of particles resides in lysosomal structures. This observation confirms results presented by Harush-Frenkel et al. (2008), who showed that anionic particles ended up in lysosomal structures, whereas cationic particles were translocated to the basolateral plasma membrane. Patterns of particles and stained lysosomes in our study were similar to patterns found by Zhang and Monteiro-Riviere (2009), who investigated several proteins and compartments relevant for endocytotic processes and found strong overlay of fluorescent quantum dots only with the lysosome markers CD63 and Lamp1.

The general pattern of particle distribution within cells, independent of particle and cell type, points towards a common determinant of particle uptake. One likely explanation is the particle stabilising effect of serum albumin, as previously reported for ceramic/metal and carbon-based nanoparticles (Deguchi et al. 2007; Bastian et al. 2009; Meißner et al. 2009). In further support of this, Yumoto et al. (2006) found that albumin co-localised with lysosomes in lung alveolar epithelial cells and microscopic patterns were similar to those observed by us. Cedervall et al. (2007) demonstrated strong binding of human serum albumin to nanoparticles and calculated an amount of about 620 albumin proteins binding at the surface of a 70 nm particle. In recent studies of our own, we calculated that the albumin content in our serum supplemented media was always higher than the potential binding ability of the particles in the concentrations applied (Meißner et al. 2010). Binding to nanoparticles of other serum proteins, such as fibrinogen and apolipoproteins, has also been reported (Cedervall et al. 2007; Lundqvist et al. 2008). Kreuter et al. (2002) demonstrated that medically used apolipoprotein-coated nanoparticles

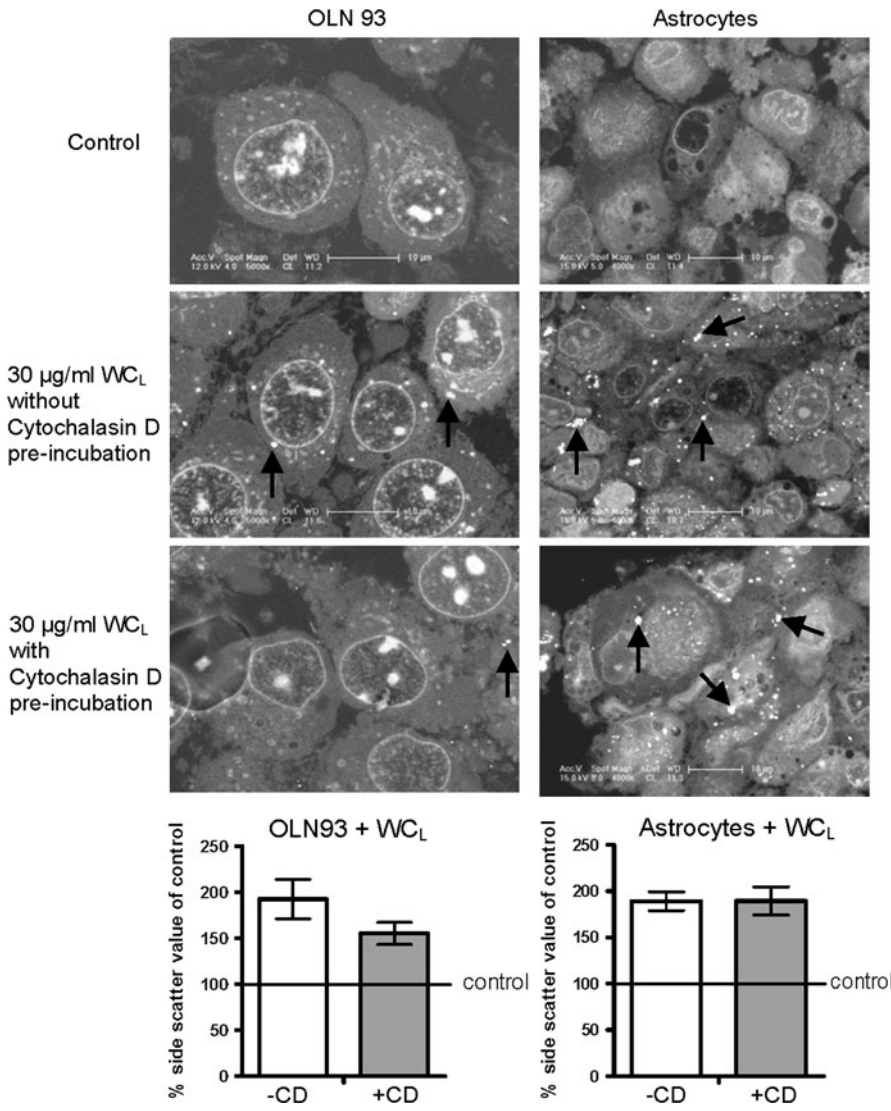

Fig. 8 SEM of OLN93 cells (*left panel*) and primary astrocytes (*right panel*) exposed to 30 µg/mL WC_L nanoparticles for 3 h with and without CytoD pre-incubation. CytoD treatment reduced particle number in OLN93 cells but not in astrocytes. *Graphs* show corresponding changes of the SSC values after identical treatments (percent of control; mean ± SE, $n = 4$)

were able to penetrate the blood brain barrier via low density lipoprotein (LDL) receptor mediated endocytosis. It thus seems that particle-bound serum proteins are not only relevant to internal exposure and systemic distribution in organisms but also influence cellular uptake and subsequent cell-internal translocation as well.

The observed co-localisation of the different particles with lysosomal structures in all cells points towards endocytosis as mechanism of particle uptake. Despite this general observation, quantification of cellular granularity by flow cytometry, measured as changes in SSC, allowed differences in uptake to be identified that were related either to cell or particle type.

With regard to cell type, primary monocytes, which are "professional" phagocytic cells, were most active in particle internalisation as demonstrated by high SSC values. All other cells responded similarly to identical particle preparations and showed significantly lower SSC signals, including cells of the monocyte cell line, THP1. Primary monocytes also differed from all other investigated cells in that particle internalisation led to the formation of large intracellular vesicles. Such vesicles are typical for phagocytosis but may themselves have contributed to increased SSC signals in a fashion unproportional to particle uptake. Primary monocytes also responded most sensitively to exposure to CytoD, an inhibitor of

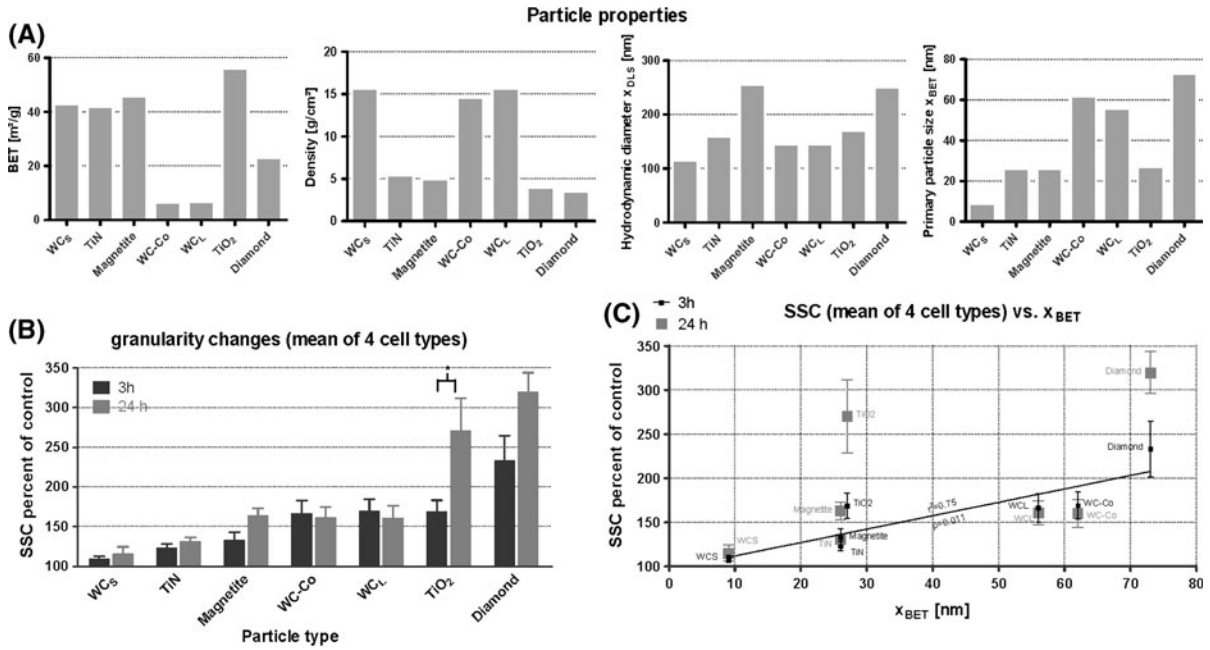

Fig. 9 Particle properties (**a**) were correlated to measured particle type dependent changes of cellular granularity, taking the mean SSC values of four cell types (HaCaT, OLN93, A549, astrocytes) after 3 and 24 h of exposure to the different nanoparticles (mean ± SE, $n \geq 4$ for each cell type) into account (**b**). A statistically significant difference between SSC values after 3 and 24 h of exposure was found only for TiO_2 particles (* $P < 0.05$, Student's t test). By comparing particle properties with SSC values only the primary particle size (x_{BET}) showed a weak correlation with SSC values after 3 h of exposure (**c**). After 24 h of exposure, a direct correlation of SSC values with any of the particle properties could not be identified

actin filaments, although CytoD also significantly inhibited nanoparticle uptake in the oligodendrocyte cell line, OLN93. Brain cells are generally able to perform phagocytosis, although this is reported more frequently for microglia and astrocytes (Thomas 1992; Roldan et al. 1997; Chang et al. 2000), the latter of which showed no impact by CytoD in this study. Actin filaments are known to be essential for phagocytosis but have been implied to play a role in other endocytic processes as well (Kaksonen et al. 2006). We therefore conclude that particle internalisation by phagocytosis was likely the main route of uptake in primary monocytes and possibly oligodendrocytes, and that other known endocytic mechanisms must have been involved in particle uptake by the other cells.

Endocytic pathways involved in nanoparticle uptake have been investigated in several studies with non-phagocytic cells (Rejman et al. 2004; Gratton et al. 2008; Harush-Frenkel et al. 2008; Oh et al. 2009; Zhang and Monteiro-Riviere 2009). All these studies evidently showed that cells use more than one pathway to internalise particles, for example by means of clathrin-mediated or caveolae-mediated endocytosis. Zhang and Monteiro-Riviere (2009) demonstrated that endosome and lysosome disrupting agents inhibited the internalisation of quantum dots into human epithelial keratinocytes, whereas CytoD had no inhibitory effects. They confirmed a specific pathway of uptake for quantum dots via lipid raft dependent and G-protein-coupled-receptor (GPCR) pathway regulated LDL/scavenger receptors. Whether similar mechanisms were involved in non-phagocytic uptake in the keratinocytes and the other cell types studied here is as yet unknown. However, two other factors need to be considered for non-phagocytic particle uptake. First, in the in vitro experiments, particles are added to the media on top of the cells and therefore gravitational forces may also play a role in particle uptake. Second, as discussed above, proteins and lipids bound to the particle surfaces may impact on the route of particle uptake. Albumin, for example, is proposed to be transported through cells via caveolae-mediated endo- and transcytosis (Schubert et al. 2001; Razani et al. 2002). However, whether a protein–particle

complex can be internalised the same way as proteins is yet unclear; certainly the nanoparticle–protein complex is much larger than a single protein.

With regard to particle type, the smallest changes of the SSC values compared to control cells were consistently found for WC_S and the highest values for diamond particles with comparable relative SSC values for each type of particle in either cell type, except for primary monocytes (see above). With respect to these findings, we conclude that cellular granularity after particle incorporation in non-phagocytic cells is much more influenced by the particle characteristics than by cell type. However, only primary particle size, x_{BET}, showed a weak correlation with early (3 h) particle uptake as quantified by SSC. Similar observations were made by Limbach et al. (2005) who showed particle size to be the dominant factor in determining the uptake of ceria nanoparticles into human lung cells. The result of a weak correlation only with primary particle size indicates that physical and/or chemical particle characteristics, not accounted for in the current study, contribute to particle uptake and the associated changes in cellular granularity. Granularity of cells is measured as intensity of the right angle scattered light and is brought about by intracellular organelles (e.g. mitochondria, nuclei) or particles that divert the incoming light in a typical pattern. It follows that, optical properties, such as reflection, refraction and absorption (Johnsen and Widder 1999), which also depend on the nanoparticles' surface and quantum effects, may influence light scattering and intensity of the SSC measurements. In support of this, TiN always resulted in much lower SSC values than TiO_2 despite a roughly similar density and particle size. TiO_2 nanoparticles are industrially used because of their white colour and the resulting optical properties (strong reflection, low absorption; absorption coefficient = 2.8 μm^{-1} for the respective wavelength of the FACS system (488 nm); http://refractiveindex.info). By contrast, TiN is a dark powder with a much higher light absorption capacity indicated by an absorption coefficient of 34.3 μm^{-1}. All other particles of the study had a dark colour, except for diamond that was grey. Thus, while changes in SSC can clearly indicate particle uptake, additional parameters and methods, such as optical properties and total element quantification by inductively coupled plasma mass spectroscopy, need to be used to link particle properties with uptake and changes in cellular granularity. Combining these approaches and applying them to a set of particles with an even broader range of particle properties to quantitatively predict particle uptake into cells will, however, be a major challenge.

In this study we unequivocally demonstrate that different types of engineered nanoparticles enter several kinds of mammalian cells. Even if found non-toxic, as demonstrated by cell viability measurements for, e.g. WC_L but not for WC–Co (Bastian et al. 2009; Kühnel et al. 2009; Busch et al. 2010), it is still unknown how cells live and deal with incorporated nanoparticles. Particles in cells may act as carriers for endogenous and exogenous substances (Baun et al. 2008; Stoeger et al. 2009), as catalysts for chemical reactions or may cause immunological responses based on recognition of the nanoparticle as a foreign entity (Ashwood et al. 2007; Kanno et al. 2007). Past experiences with several kinds of lung diseases caused by fibres and industrial dusts, often appearing long time after exposure, support concerns about engineered nanoparticles (Maynard and Kuempel 2005). Therefore, the long-term fate of technical nanoparticles in cells in vitro and in vivo needs to be identified. Considering the ability of technical nanoparticles to enter various kinds of cells, in conjunction with our currently limited knowledge regarding the intracellular nanoparticle fate, occupational and consumer exposure should be minimised.

Acknowledgements This research was supported by the German Federal Ministry for Education and Research (BMBF) within the INOS project (Identification and Evaluation of Health and Environmental Effects of Technical Particles at the Nanoscale; Grant #03X0013C), WB was additionally supported by the Max Buchner Forschungsstiftung and by the Helmholtz Impulse and Networking Fund through Helmholtz Interdisciplinary Graduate School for Environmental Research (HIGRADE). Stefan Scholz (Department Bioanalytical Ecotoxicology, UFZ) is acknowledged for constructive discussions.

References

Ashwood P, Thompson RP, Powell JJ (2007) Fine particles that adsorb lipopolysaccharide via bridging calcium cations may mimic bacterial pathogenicity towards cells. Exp Biol Med 232:107–117

Bao L, Chen S, Wu L, Hei TK, Wu Y, Yu Z, Xu A (2007) Mutagenicity of diesel exhaust particles mediated by cell–particle interaction in mammalian cells. Toxicology 229:91–100

Bastian S, Busch W, Kühnel D, Springer A, Meißner T, Holke R, Scholz S, Iwe M, Pompe W, Gelinsky M, Potthoff A, Richter V, Ikonomidou C, Schirmer K (2009) Toxicity of tungsten carbide and cobalt-doped tungsten carbide nanoparticles in mammalian cells in vitro. Environ Health Perspect 117:530–536

Baun A, Sorensen SN, Rasmussen RF, Hartmann NB, Koch CB (2008) Toxicity and bioaccumulation of xenobiotic organic compounds in the presence of aqueous suspensions of aggregates of nano-C(60). Aquat Toxicol 86:379–387

Bhattacharya K, Davoren M, Boertz J, Schins R, Hoffmann E, Dopp E (2009) Titanium dioxide nanoparticles induce oxidative stress and DNA-adduct formation but not DNA-breakage in human lung cells. Part Fibre Toxicol 6:17

Busch W, Kühnel D, Schirmer K, Scholz S (2010) Tungsten carbide cobalt nanoparticles exert hypoxia-like effects on the gene expression level in human keratinocytes. BMC Genomics 11:65

Cedervall T, Lynch I, Lindman S, Berggard T, Thulin E, Nilsson H, Dawson KA, Linse S (2007) Understanding the nanoparticle–protein corona using methods to quantify exchange rates and affinities of proteins for nanoparticles. Proc Natl Acad Sci USA 104:2050–2055

Chang GH, Barbaro NM, Pieper RO (2000) Phosphatidylserine-dependent phagocytosis of apoptotic glioma cells by normal human microglia, astrocytes, and glioma cells. Neuro Oncol 2:174–183

Chen M, von Mikecz A (2005) Formation of nucleoplasmic protein aggregates impairs nuclear function in response to SiO_2 nanoparticles. Exp Cell Res 305:51–62

Chithrani BD, Ghazani AA, Chan WC (2006) Determining the size and shape dependence of gold nanoparticle uptake into mammalian cells. Nano Lett 6:662–668

Deguchi S, Yamazaki T, Mukai SA, Usami R, Horikoshi K (2007) Stabilization of C60 nanoparticles by protein adsorption and its implications for toxicity studies. Chem Res Toxicol 20:854–858

Geiser M, Rothen-Rutishauser B, Kapp N, Schurch S, Kreyling W, Schulz H, Semmler M, Im Hof V, Heyder J, Gehr P (2005) Ultrafine particles cross cellular membranes by nonphagocytic mechanisms in lungs and in cultured cells. Environ Health Perspect 113:1555–1560

Gojova A, Guo B, Kota RS, Rutledge JC, Kennedy IM, Barakat AI (2007) Induction of inflammation in vascular endothelial cells by metal oxide nanoparticles: effect of particle composition. Environ Health Perspect 115:403–409

Gratton SE, Ropp PA, Pohlhaus PD, Luft JC, Madden VJ, Napier ME, DeSimone JM (2008) The effect of particle design on cellular internalization pathways. Proc Natl Acad Sci USA 105:11613–11618

Haberzettl P, Duffin R, Kramer U, Hohr D, Schins RP, Borm PJ, Albrecht C (2007) Actin plays a crucial role in the phagocytosis and biological response to respirable quartz particles in macrophages. Arch Toxicol 81:459–470

Harush-Frenkel O, Rozentur E, Benita S, Altschuler Y (2008) Surface charge of nanoparticles determines their endocytic and transcytotic pathway in polarized MDCK cells. Biomacromolecules 9:435–443

Hildebrand H, Kühnel D, Potthoff A, Mackenzie K, Springer A, Schirmer K (2009) Evaluating the cytotoxicity of palladium/magnetite nano-catalysts intended for wastewater treatment. Environ Pollut 158:65–73

Johnsen S, Widder EA (1999) The physical basis of transparency in biological tissue: ultrastructure and the minimization of light scattering. J Theor Biol 199:181–198

Kaksonen M, Toret CP, Drubin DG (2006) Harnessing actin dynamics for clathrin-mediated endocytosis. Nat Rev Mol Cell Biol 7:404–414

Kanno S, Furuyama A, Hirano S (2007) A murine scavenger receptor MARCO recognizes polystyrene nanoparticles. Toxicol Sci 97:398–406

Kreuter J, Shamenkov D, Petrov V, Ramge P, Cychutek K, Koch-Brandt C, Alyautdin R (2002) Apolipoprotein-mediated transport of nanoparticle-bound drugs across the blood–brain barrier. J Drug Target 10:317–325

Kühnel D, Busch W, Meißner T, Springer A, Potthoff A, Richter V, Gelinsky M, Scholz S, Schirmer K (2009) Agglomeration of tungsten carbide nanoparticles in exposure medium does not prevent uptake and toxicity toward a rainbow trout gill cell line. Aquat Toxicol 93:91–99

Limbach LK, Li Y, Grass RN, Brunner TJ, Hintermann MA, Muller M, Gunther D, Stark WJ (2005) Oxide nanoparticle uptake in human lung fibroblasts: effects of particle size, agglomeration, and diffusion at low concentrations. Environ Sci Technol 39:9370–9376

Long TC, Saleh N, Tilton RD, Lowry GV, Veronesi B (2006) Titanium dioxide (P25) produces reactive oxygen species in immortalized brain microglia (BV2): implications for nanoparticle neurotoxicity. Environ Sci Technol 40:4346–4352

Lundqvist M, Stigler J, Elia G, Lynch I, Cedervall T, Dawson KA (2008) Nanoparticle size and surface properties determine the protein corona with possible implications for biological impacts. Proc Natl Acad Sci USA 105:14265–14270

Maynard AD, Kuempel ED (2005) Airborne nanostructured particles and occupational health. J Nanopart Res 7: 587–614

Meißner T, Potthoff A, Richter V (2009) Physico-chemical characterization in the light of toxicological effects. Inhal Toxicol 21(Suppl 1):35–39

Meißner T, Kühnel D, Busch W, Oswald S, Richter V, Michaelis A, Schirmer K, Potthoff A (2010) Physical–chemical characterization of tungsten carbide nanoparticles as a basis for toxicological investigations. Nanotoxicology 4:196–206

Naß R, Albayrak S, Aslan M, Schmidt H (1994) Colloidal processing and sintering of nano-scale TiN. In: 5th international conference in ceramic processing, science and technology. Friedrichshafen, Germany

Oh JM, Choi SJ, Lee GE, Kim JE, Choy JH (2009) Inorganic metal hydroxide nanoparticles for targeted cellular uptake through clathrin-mediated endocytosis. Chem Asian J 4:67–73

Papis E, Rossi F, Raspanti M, Dalle-Donne I, Colombo G, Milzani A, Bernardini G, Gornati R (2009) Engineered cobalt oxide nanoparticles readily enter cells. Toxicol Lett 189:253–259

Potthoff A, Meißner T, Richter V, Busch W, Kühnel D, Bastian S, Iwe M, Springer A (2009) Evaluation of health risks of

nanoparticles—a contribution to a sustainable development of nanotechnology. Solid State Phenom 151:183–189

Razani B, Woodman SE, Lisanti MP (2002) Caveolae: from cell biology to animal physiology. Pharmacol Rev 54:431–467

Rejman J, Oberle V, Zuhorn IS, Hoekstra D (2004) Size-dependent internalization of particles via the pathways of clathrin- and caveolae-mediated endocytosis. Biochem J 377:159–169

Reyes L, Davidson MK, Thomas LC, Davis JK (1999) Effects of Mycoplasma fermentans incognitus on differentiation of THP-1 cells. Infect Immun 67:3188–3192

Roldan A, Gogg S, Ferrini M, Schillaci R, De Nicola AF (1997) Glucocorticoid regulation of in vitro astrocyte phagocytosis. Biocell 21:83–89

Schubert W, Frank PG, Razani B, Park DS, Chow CW, Lisanti MP (2001) Caveolae-deficient endothelial cells show defects in the uptake and transport of albumin in vivo. J Biol Chem 276:48619–48622

Spurr AR (1969) A low-viscosity epoxy resin embedding medium for electron microscopy. J Ultrastruct Res 26:31–43

Stearns R, Paulauskis J, Godleski J (2001) Endocytosis of ultrafine particles by A549 cells. Am J Respir Cell Mol Biol 24:108–115

Stoeger T, Takenaka S, Frankenberger B, Ritter B, Karg E, Maier K, Schulz H, Schmid O (2009) Deducing in vivo toxicity of combustion-derived nanoparticles from a cell-free oxidative potency assay and metabolic activation of organic compounds. Environ Health Perspect 117:54–60

Stringer B, Imrich A, Kobzik L (1995) Flow cytometric assay of lung macrophage uptake of environmental particulates. Cytometry 20:23–32

Thomas EW (1992) Brain macrophages: evaluation of microglia and their functions. Brain Res Rev 17:61–74

Xia T, Kovochich M, Brant J, Hotze M, Sempf J, Oberley T, Sioutas C, Yeh JI, Wiesner MR, Nel AE (2006) Comparison of the abilities of ambient and manufactured nanoparticles to induce cellular toxicity according to an oxidative stress paradigm. Nano Lett 6:1794–1807

Yumoto R, Nishikawa H, Okamoto M, Katayama H, Nagai J, Takano M (2006) Clathrin-mediated endocytosis of FITC-albumin in alveolar type II epithelial cell line RLE-6TN. Am J Physiol Lung Cell Mol Physiol 290:L946–L955

Zhang LW, Monteiro-Riviere NA (2009) Mechanisms of quantum dot nanoparticle cellular uptake. Toxicol Sci 110:138–155